

Quasiparticle bands and spectra of Ga₂O₃ polymorphs

J. Furthmüller and F. Bechstedt

*Institut für Festkörpertheorie und -optik and European Theoretical Spectroscopy Facility,
Friedrich-Schiller-Universität Jena, Max-Wien-Platz 1, D-07743 Jena, Germany*

(Received 11 November 2015; published 15 March 2016)

Within the framework of density functional theory and Hedin's *GW* approximation for single-particle excitations, we present quasiparticle band structures and densities of states for two gallium oxide polymorphs: rhombohedral α -Ga₂O₃ and monoclinic β -Ga₂O₃. The gap problem is attacked. In addition, their electron effective mass tensors are given. Solving the Bethe-Salpeter equation we also calculate excitonic optical spectra of the two polymorphs. The treatment of excitonic effects allows for a trustable prediction of optical properties from the band gap to the ultraviolet region. In addition, for few other polymorphs we also discuss the frequency-dependent dielectric tensor within the independent-particle approximation (random phase approximation) and densities of states on density functional level. We demonstrate that apart from subtle details, the overall densities of states and optical spectra, in particular the isotropically averaged spectra, are rather similar for all polymorphs, while the electronic dielectric constants vary with the structure. For all polymorphs, complete sets of elastic constants are given.

DOI: [10.1103/PhysRevB.93.115204](https://doi.org/10.1103/PhysRevB.93.115204)

I. INTRODUCTION

Gallium oxide is a transparent conducting oxide which gained increasing interest in recent years due to its high electrical conductivity [1] and transparency in the ultraviolet (UV) region. This makes it a promising material for transparent electronic [1,2] and optoelectronic [3] but also conventional electronic devices as field effect transistors [4]. The interest in its electronic and optical properties has recently increased because of its potential application as an UV transparent conducting oxide (TCO) [5,6]. Such a TCO is widely used as transparent electrodes for flat panel displays and solar cells. Despite its widespread applications, the fundamental properties are poorly understood. Among the experimental obstacles are the difficulties in preparing single crystals and thin films with sufficient quality. The difficulties of a theoretical, especially *ab initio*, treatment are mainly due to many atoms in the unit cell and, hence, many structural degrees of freedom.

Another difficulty is the fact that gallium oxide exhibits a pronounced polymorphism similar to aluminum oxide or indium oxide. Already in 1952 Roy *et al.* reported the existence of five different polymorphs of Ga₂O₃ [7]. In 2008, Yusa *et al.* claimed even the possibility of a sixth polymorph [8]. The TCO Ga₂O₃ crystallizes in monoclinic (β -Ga₂O₃), rhombohedral (α -Ga₂O₃), defective spinel (γ -Ga₂O₃), cubic (δ -Ga₂O₃), or orthorhombic (ϵ -Ga₂O₃) structure. In particular, a theoretical study based on density functional theory (DFT) of Yoshioka *et al.* [9] shed light on the different structures and their thermodynamic stability. Overall, there exist already many DFT studies for Ga₂O₃, not only about structural properties but also about band structures (employing DFT or the B3LYP hybrid functional [10]) and optical properties [11,12], or employing a scissors operator correction for the band gap and for optical spectra [13]. However, these DFT studies are by far not complete. Although hybrid functionals as B3LYP may give improved band structures, it is well known that DFT eigenvalues do not include any excitation aspect and even hybrid functionals mimic excitation aspects only partly in a

very crude approximation. Also independent-particle optical spectra do not reflect measured spectra at all because they lack excitonic effects. The DFT results cannot explain the measured data, especially not the fundamental gap. However, also the experimental studies of β -Ga₂O₃ exhibit features in optical absorption and angular-resolved photoelectron spectroscopy (ARPES) which are controversially discussed, in particular, in the context of the gap [14–17].

The DFT studies may give a first impression and general trends but no final answer yet. Apart from one exception [18], there exist no studies on a more elaborate many-body level like Hedin's *GW* approach [19] for the band structures or calculations of full excitonic spectra solving the Bethe-Salpeter equation (BSE) of many-body perturbation theory (MBPT) [20,21]. But, even the study of Varley *et al.* [18] treated the band structure only on the level of DFT plus a scissors shift for the band-gap correction. Their BSE calculation was only based on an approximate screened Coulomb potential *W* employing a simple model screening. The variety of the optical spectra, especially not with respect to the low crystal symmetry, has not been considered. Only the imaginary parts of the diagonal components of the dielectric tensor were displayed. In this paper, we present a fully elaborated study employing DFT, *GW*, and BSE calculations for different polymorphs of Ga₂O₃. In particular, quasiparticle band structures and spectra for the complete dielectric tensor are calculated. After a short description of the theoretical and computational methods in Sec. II, results are presented in Secs. III (structural and elastic properties), IV (band structures), and V (optical spectra). Finally, in Sec. VI a brief summary and conclusions are given.

II. COMPUTATIONAL DETAILS

All calculations have been carried out with the Vienna *ab initio* simulation package (VASP) [22] within the framework of DFT and MBPT. For all ground-state calculations, we employed the so-called AM05 [23] generalized gradient approximation (GGA) to describe exchange and correlation. It has been demonstrated that this exchange-correlation

functional gives rise to atomic geometries of wide-gap semiconductors with strong ionic bonds in excellent agreement with measured values [24]. For single-quasiparticle band structure calculations we used Hedin's GW [19] approach in order to account for the excitation aspects which are lacking within the DFT-GGA approach [21]. In order to improve the quality of the starting electronic wave functions and the dielectric function entering the screened Coulomb interaction W for the single-shot G_0W_0 calculation, we use a HSE06 [25] hybrid functional electronic structure calculation as a starting point instead of a DFT starting point. In addition, we have altered the original HSE06 reciprocal screening length from about 0.2 \AA^{-1} to 0.3 \AA^{-1} as suggested and well tested in a study of Fuchs *et al.* [26]. After tests with up to 768 bands, 512 bands are used in the GW self-energy calculation. The frequency-dependent dielectric tensor is computed by solving the BSE introducing a two-particle Hamiltonian which accounts for the excitonic effects, screened electron-hole attraction and bare electron-hole exchange [21,27]. The screened potential W is taken from the GW calculations. For the BSE calculations, the number of bands has been limited to the possibility to describe energy distances between conduction and valence bands up to 28 eV ($8 \times 8 \times 8$ \mathbf{k} points) and 44 eV ($6 \times 6 \times 6$ \mathbf{k} points). The resulting excitonic Hamiltonians have ranks up to about 433 000. Therefore, the imaginary part of the dielectric tensor is computed using a time-propagation technique [28]. A Lorentzian broadening of 0.2 eV width has been used for all spectra to simulate lifetimes of excitons and possible instrumental broadenings.

We use the frozen-core all-electron projector-augmented wave (PAW) method [29,30] to describe wave functions and potentials. A plane-wave cutoff energy for the expansion of the pseudopartial waves of 410 eV (about 30 Ry) has been chosen for all total-energy, band structure, and spectra calculations. This cutoff energy has been proven to provide a very good accuracy for total energies (better about 1 meV/atom). Due to the fact that several polymorphs possess a rather complicated crystallographic structure (e.g., base-centered monoclinic for the ground-state structure, see following section), it is much too time consuming to sample the total-energy surface for a sufficiently large set of a , b , and c lattice constants and in addition also some monoclinic angle β . Therefore, we employ a much more efficient strategy: For several volumes we use the built-in stress tensor to fully relax not only the atomic coordinates, but also the full cell *shape*. This is then followed by a simple energy-volume fit using Vinet's equation of state [31]. A pre-estimate of the equilibrium volume is achieved by a full relaxation including also volume relaxation. In order to avoid spurious Pulay stresses [32], such kind of relaxation strategies formally require *absolute* convergence with respect to the plane-wave cutoff energy or at least a very high cutoff. For that reason, all structural optimizations have been performed with an increased plane-wave cutoff energy of 820 eV (about 60 Ry). Tests for varying cutoffs (up to 950 eV) have proven that the estimated error should be less than 1 kbar in the stresses leaving a maximum uncertainty in the lattice constants of 0.1% or less (or few mÅ in absolute numbers). All structures have been relaxed until the forces on the atoms dropped below 1 meV/Å and the anisotropy of the stress tensor was less than 0.1 kbar.

The k -point sampling of the Brillouin zone (BZ) was performed using standard Monkhorst-Pack [33] meshes for all structural relaxations. We use a mesh size of $11 \times 11 \times 11$ ($9 \times 9 \times 5$, $4 \times 4 \times 4$) for the monoclinic and rhombohedral (orthorhombic, cubic) structures. For band structure calculations we used Γ -centered Monkhorst-Pack meshes. The mesh sizes were $16 \times 16 \times 16$ ($16 \times 8 \times 8$, $8 \times 8 \times 8$) for the monoclinic and rhombohedral (orthorhombic, cubic) structures in the DFT case and $8 \times 8 \times 8$ for the HSE06, GW , and BSE calculations in the case of the monoclinic and rhombohedral structures. For the high-energy tails of the dielectric tensor on BSE level beyond transition energies of 28 eV we reduce the mesh size to $6 \times 6 \times 6$. For the complex orthorhombic and cubic structures, we do not perform any GW calculations because it would be too time consuming and the monoclinic and rhombohedral phases are the only ones which can be studied under ambient conditions (whereof the monoclinic one is the only stable phase).

III. STRUCTURAL, ELASTIC, AND ENERGETIC PROPERTIES

A. Phases

According to the Introduction, there exist at least five or even six polymorphs of Ga_2O_3 . We study four polymorphs: (i) the base-centered monoclinic β phase which is the only stable phase up to at least $T = 1800^\circ\text{C}$, (ii) the metastable rhombohedral corundum structure, also called α phase, which is the only metastable phase that can exist under ambient conditions, (iii) the cubic bixbyite structure, also called δ phase, and (iv) the orthorhombic ϵ phase. The β phase can be transformed into the α phase under hydrostatic pressure at higher temperatures [34,35]. The cubic bixbyite polymorph is the ground-state structure in the case of In_2O_3 [36]. The ϵ phase was found to appear by heating δ - Ga_2O_3 . For the ϵ phase we only discuss the structure proposed by Yoshioka *et al.* [9] although another orthorhombic high-pressure phase which could be a $\text{Rh}_2\text{O}_3(\text{II})$ -type structure was suggested by Yusa *et al.* [8]. The so-called γ phase, suggested to be a defective spinel-type structure [9], is not examined due to its high complexity in the description. Yoshioka *et al.* [9] optimized the geometry of the γ - Ga_2O_3 within 14 inequivalent configurations of defective spinel structure.

As we will demonstrate later, all polymorphs have a lot in common concerning the electronic structure or dielectric properties [similar densities of states (DOS) and similar isotropically averaged dielectric functions], apart from a varying fundamental band gap. As illustrated and described in the papers of Geller [37] and Ahman *et al.* [38] (see Fig. 1 therein), one can build up the crystal structures by different arrangements of oxygen octahedra and tetrahedra as building blocks. The occurrence of the same building blocks seems to be the origin of similar electronic and optical properties and is the main issue of this paper. At the end our main focus will be given to the α and β phases only.

The most important characteristics of the ground states of the four polymorphs under consideration, i.e., all unit-cell parameters (lattice constants and angles), atomic coordinates, space group, bulk moduli, pressure derivatives of bulk moduli,

TABLE I. Calculated key structural and thermodynamic data of the four polymorphs under consideration. Known experimental data from Ref. [34] are given in parentheses. The cohesive energy E_0 is taken relative to the energies of free spin-polarized atoms. An experimental value of $E_0 \approx -24.7$ eV is estimated at room temperature combining heats of formation of β -Ga₂O₃, O₂ molecules, and Ga bulk (extracted from Ref. [39]). It is expected that neglecting phonon free energies the experimental zero-temperature value without phonon zero-point motion energies (neglected in all calculations) should be most likely about -24.9 eV.

| Phase | β | α | δ | ϵ |
|--------------------------------------|------------------|------------------|-------------|------------|
| Bravais lattice | Monocl. | Trigonal | Cubic | Orthorh. |
| Space group | $C2/m$ | $R\bar{3}c$ | $Ia\bar{3}$ | $Pna2_1$ |
| Atoms per unit cell | 10 | 10 | 40 | 40 |
| V_0 (Å ³ /formula unit) | 52.84 (52.39) | 48.48 (48.07) | 50.14 | 51.09 |
| B_0 (elastic tensor) (MBar) | 1.66 | 2.16 | 1.95 | 1.85 |
| B_0 (fit) (MBar) | 1.65 (1.99) | 2.15 (2.20) | 1.93 | |
| B'_0 | 3.8 (3.1) | 4.5 (5.9) | 4.7 | |
| E_0 (eV/formula unit) | -25.343 | -25.254 | -25.213 | -25.262 |

and cohesive energies are summarized in Table I. In this table, we list first the general cohesive properties for all polymorphs under consideration. In Tables II–V we summarize then the detailed crystallographic data of the four polymorphs and the calculated structural parameters (lattice parameters and atomic positions).

The energy gain due to chemical bonding per formula unit Ga₂O₃ in Table I only weakly varies with the phase by less than 0.14 eV. The β phase is the most favored one, while the cubic bixbyite structure is less stable compared to the other Ga₂O₃ polymorphs. The most favorable β phase is the most less dense arrangement of the Ga and O atoms. Correspondingly, the bulk modulus B_0 and its pressure derivative B'_0 possess the smallest values. These trends are in agreement with the

TABLE II. Lattice parameters (a) and atomic coordinates (b) of the base-centered monoclinic structure with space group $C2/m$ (space group 12).

| Atom | (a) | | | β (°) |
|-------------------|---------|---------|---------|-------------|
| | a (Å) | b (Å) | c (Å) | |
| This work | 12.2894 | 3.0471 | 5.8113 | 103.77 |
| Ref. [9] | 12.438 | 3.084 | 5.877 | 103.71 |
| Expt. (Ref. [34]) | 12.233 | 3.038 | 5.807 | 103.82 |

| Atom | (b) | | Symmetry degeneracy |
|-----------------|-----------------------|----------|---------------------|
| | Structural parameters | | |
| | x | z | |
| Ga ₁ | 0.34192 | -0.31441 | 2 |
| Ga ₂ | 0.09016 | -0.20508 | 2 |
| O ₁ | 0.17344 | -0.43589 | 2 |
| O ₂ | 0.16329 | 0.10955 | 2 |
| O ₃ | 0.49574 | 0.25595 | 2 |

TABLE III. Lattice parameters (a) and atomic coordinates (b) of the rhombohedral corundum structure with space group $R\bar{3}c$ (space group 167).

| Atom | (a) | | | Symmetry degeneracy |
|-------------------|---------|--------------|----------------------|---------------------|
| | a (Å) | α (°) | a_{hex} (Å) | |
| This work | 5.3307 | 55.905 | 4.997 | 13.447 |
| Ref. [9] | 5.398 | 55.889 | 5.059 | 13.618 |
| Expt. (Ref. [34]) | 5.321 | 55.795 | 4.979 | 13.432 |

| Atom | (b) | | Symmetry degeneracy |
|-----------------|-----------------------|---------|---------------------|
| | Structural parameters | | |
| | x | z | |
| Ga ₁ | | 0.14396 | 4 |
| O ₁ | -0.05317 | | 6 |

experimental findings [34] for the α and β phases. The B values of In₂O₃ polymorphs are between those of the α - and β -Ga₂O₃ [36], whereas metal monoxides usually exhibit smaller elastic moduli [40].

The calculated total-energy curves $E = E(V)$ used to derive the parameters V_0 , B_0 , B'_0 , and $E_0 = E(V_0)$ listed in Table I allow the discussion of structural changes in form of pressure-induced phase transitions via the enthalpy $H = E + pV$ as a function of the hydrostatic pressure p [40]. The crossing between the $H = H(p)$ curves for two phases defines the transition pressure p_t . We obtain the value $p_t = 3.4$ GPa for the pressure-induced phase transition between the β phase and α -Ga₂O₃. This value is not too far away from the experimentally determined transition pressures at high temperatures $p_t = 4.4$ GPa [35], but clearly lower than $p_t = 19.2$ GPa reported under cold compression [41].

B. Atomic coordinates

The lattice vectors of the base-centered monoclinic β phase are given by

$$\begin{aligned}
 \mathbf{a}_1 &= (a/2, -b/2, 0), \\
 \mathbf{a}_2 &= (a/2, b/2, 0), \\
 \mathbf{a}_3 &= (c \cos \beta, 0, c \sin \beta).
 \end{aligned} \tag{1}$$

Calculated values at zero pressure and zero temperature are given in Table II(a).

All atoms have Wyckoff positions $4i$. Each Wyckoff position $4i$ results in two symmetry-equivalent lattice coordinates $\pm(x\mathbf{a}_1 + x\mathbf{a}_2 + z\mathbf{a}_3)$. The primitive unit cell contains 10 atoms at five different Wyckoff positions which are characterized by 10 different structural parameters

TABLE IV. Atomic coordinates of the body-centered-cubic bixbyite structure with space group $Ia\bar{3}$ (space group 206).

| Atom | Lattice coordinates | | | | Symmetry degeneracy |
|-------------------|---------------------|---------|---------|---------|---------------------|
| | x_1 | x_2 | y_2 | z_2 | |
| Ga _{24d} | 0.46417 | | | | 12 |
| O ₁ | | 0.38917 | 0.15795 | 0.38497 | 24 |

TABLE V. Lattice parameters (a) and atomic coordinates (b) of the orthorhombic structure with space group $Pna2_1$ (space group 33).

| (a) | | | | |
|-----------------|-----------------------|---------|---------|---------------------|
| | a (Å) | b (Å) | c (Å) | |
| This work | 5.0566 | 8.6867 | 9.3035 | |
| Ref. [9] | 5.120 | 8.792 | 9.410 | |
| (b) | | | | |
| Atom | Structural parameters | | | Symmetry degeneracy |
| | x | y | z | |
| Ga ₁ | 0.1793 | 0.1520 | 0.9982 | 4 |
| Ga ₂ | 0.8122 | 0.1616 | 0.3095 | 4 |
| Ga ₃ | 0.1916 | 0.1505 | 0.5872 | 4 |
| Ga ₄ | 0.6789 | 0.0322 | 0.7954 | 4 |
| O ₁ | 0.9711 | 0.3246 | 0.4262 | 4 |
| O ₂ | 0.5217 | 0.4885 | 0.4330 | 4 |
| O ₃ | 0.6511 | 0.0017 | 0.2041 | 4 |
| O ₄ | 0.1533 | 0.1585 | 0.1977 | 4 |
| O ₅ | 0.8486 | 0.1709 | 0.6702 | 4 |
| O ₆ | 0.5208 | 0.1678 | 0.9382 | 4 |

$x_1, x_2, x_3, x_4, x_5, z_1, z_2, z_3, z_4,$ and z_5 . The parameters x and z for the 10 atoms in the unit cell are listed in Table II(b).

The lattice vectors of the rhombohedral α phase can be chosen as

$$\mathbf{a}_1 = (b', a', a'), \quad \mathbf{a}_2 = (a', b', a'), \quad \mathbf{a}_3 = (a', a', b'). \quad (2)$$

It should be noted that this does not refer to the usual standard setting but is a choice that includes the special cases of standard cubic lattice vectors for special choices of b' and a' , i.e., special rhombohedral angles. Thereby, the rhombohedral lattice constant (length of each vector) is $a = \sqrt{2a'^2 + b'^2}$ and the rhombohedral angle α between the lattice vectors is $\alpha = \arccos([a'^2 + 2a'b']/a^2)$. Often also an equivalent nonprimitive hexagonal cell containing three primitive cells is used to characterize the structure. The corresponding hexagonal lattice constants are $a_{\text{hex}} = a\sqrt{2[1 - \cos(\alpha)]}$ and $c_{\text{hex}} = a\sqrt{3[1 + 2\cos(\alpha)]}$. Calculated values at zero pressure and zero temperature are listed in Table III(a).

All Ga atoms have Wyckoff positions $4c$. Each Wyckoff position $4c$ results in four symmetry-related lattice coordinates $\pm z(\mathbf{a}_1 + \mathbf{a}_2 + \mathbf{a}_3)$ and $\pm(0.5 + z)(\mathbf{a}_1 + \mathbf{a}_2 + \mathbf{a}_3)$. All O atoms have Wyckoff positions $6e$. Each Wyckoff position $6e$ results in six symmetry-related lattice coordinates of the form $\pm[x\mathbf{a}_1 + (0.5 - x)\mathbf{a}_2 + 0.25\mathbf{a}_3]$ with three cyclic permutations of the coefficients $x, (0.5 - x),$ and 0.25 . The primitive unit cell contains 10 atoms with exactly one Wyckoff position for Ga and O which are characterized by two different structural parameters z_1 and x_1 given in Table III(b).

The lattice vectors of the cubic δ phase are given by

$$\begin{aligned} \mathbf{a}_1 &= (-a/2, a/2, a/2), \\ \mathbf{a}_2 &= (a/2, -a/2, a/2), \\ \mathbf{a}_3 &= (a/2, a/2, -a/2). \end{aligned} \quad (3)$$

Calculated values at zero pressure and zero temperature are $a = 9.292 \text{ \AA}$ (this work) and $a = 9.401 \text{ \AA}$ (Ref. [9]).

There are four Ga atoms at four different Wyckoff positions $8b$ which are $0.5(\mathbf{a}_1 + \mathbf{a}_2 + \mathbf{a}_3), 0.5\mathbf{a}_1, 0.5\mathbf{a}_2,$ and $0.5\mathbf{a}_3$. All other Ga atoms occupy Wyckoff positions $24d$. Each Wyckoff position $24d$ results in 12 symmetry-related lattice coordinates of the form $\pm[0.25\mathbf{a}_1 + (x + 0.25)\mathbf{a}_2 + x\mathbf{a}_3]$ and $\pm[0.25\mathbf{a}_1 + (x - 0.25)\mathbf{a}_2 + (x + 0.5)\mathbf{a}_3]$ with three cyclic permutations each of the coefficients $0.25, (x + 0.25),$ and x or, respectively, $0.25, (x - 0.25),$ and $(x + 0.5)$. All O atoms have Wyckoff positions $48e$. Each Wyckoff position $48e$ results in 24 symmetry-related lattice coordinates of the four fundamental forms $\pm[(x + y)\mathbf{a}_1 + (y + z)\mathbf{a}_2 + (x + z)\mathbf{a}_3], \pm[(0.5 - x - y)\mathbf{a}_1 + (0.5 - y + z)\mathbf{a}_2 + (z - x)\mathbf{a}_3], \pm[(0.5 - x + y)\mathbf{a}_1 + (y - z)\mathbf{a}_2 + (0.5 - x - z)\mathbf{a}_3],$ and $\pm[(x - y)\mathbf{a}_1 + (0.5 - y - z)\mathbf{a}_2 + (0.5 + x - z)\mathbf{a}_3]$ with again three cyclic permutations each of the coefficients in front of $\mathbf{a}_1, \mathbf{a}_2,$ and \mathbf{a}_3 . In total, the primitive unit cell contains 40 atoms. The Wyckoff positions $8b$ of four Ga atoms do not possess any structural parameters, the Wyckoff position $24d$ of the remaining 16 Ga atoms can be characterized by a single parameter x_1 . For the O atoms at Wyckoff position $48e$ we need another three parameters $x_2, y_2,$ and z_2 . The corresponding parameters are listed in Table IV.

The lattice vectors of the orthorhombic ϵ phase are given by

$$\mathbf{a}_1 = (a, 0, 0), \quad \mathbf{a}_2 = (0, b, 0), \quad \mathbf{a}_3 = (0, 0, c). \quad (4)$$

Calculated values at zero pressure and zero temperature are listed in Table V(a).

There are 16 Ga atoms at four different Wyckoff positions $4a$ and 24 O atoms at six different Wyckoff positions $4a$. Each Wyckoff positions $4a$ results in four symmetry-related lattice coordinates of the form $x\mathbf{a}_1 + y\mathbf{a}_2 + z\mathbf{a}_3, (0.5 + x)\mathbf{a}_1 + (0.5 - y)\mathbf{a}_2 + z\mathbf{a}_3, (0.5 - x)\mathbf{a}_1 + (0.5 + y)\mathbf{a}_2 + (0.5 + z)\mathbf{a}_3,$ and $-x\mathbf{a}_1 - y\mathbf{a}_2 + (0.5 + z)\mathbf{a}_3$. The parameters $x, y,$ and z are given in Table V(b).

The calculated lattice constants for the four considered polymorphs qualitatively agree with previous results [9]. However, our values are smaller as a consequence of the use of the PBE approximation for exchange and correlation [42] by Yoshioka *et al.* [9]. This discrepancy has been also found for polymorphs of mononitrides [24] with a clear tendency that the lattice constants obtained in the AM05 framework are much closer to measured values. This observation is supported by Tables II(a) and III(a), which show that our AM05 values better describe the measured values. Consequently, the predictions for the δ and ϵ phases should be reasonable. The rhombohedral (α) and monoclinic (β) angles are in excellent agreement with other calculated [9] and measured [34] values. The atomic coordinates in Tables II(b), III(b), IV, and V(b) agree well with the results of Yoshioka *et al.* [9]. Summarizing, we conclude that the atomic geometries in Tables II, III, IV, and V of the four polymorphs under consideration are suitable for the calculation of the electronic and optical properties.

C. Tensor of elastic constants

For the four polymorphs under consideration, we also determine the full tensor of elastic constants which, to our knowledge, is completely unknown so far. This can be

achieved by calculation of the stress-strain relation for different deformation modes of the unit cell. Thereby, also cell-internal stress contributions due to atomic relaxations have been taken into account. In order to avoid too large errors due to Pulay stresses [32], these calculations have again been performed at an increased plane-wave cutoff of 820 eV. Four deformation amplitudes per degree of freedom (two in positive and two in negative directions) plus the equilibrium position have been used in order to determine the second derivatives of the stress with respect to strain at the equilibrium positions. In the following, we refer to the frequently used Voigt notation which allows to represent the tensor of elastic constants C_{ijkl} as a (symmetric) 6×6 matrix C_{ij} , with a maximum of 21 independent elements. The mapping of indices is $11 \rightarrow 1$, $22 \rightarrow 2$, $33 \rightarrow 3$, $23 \rightarrow 4$, $31 \rightarrow 5$, and $12 \rightarrow 6$.

In the monoclinic case, one finds 13 independent elastic moduli by symmetry reduction. Choosing the coordinate system such that the y axis is parallel to the b axis, x is parallel to the a axis, and the c axis is in the xz plane [according to the choice of lattice vectors in Eq. (1)], symmetry enforces $C_{14} = C_{24} = C_{34} = C_{16} = C_{26} = C_{36} = C_{45} = C_{54} = C_{56} = C_{65} = 0$. In units of kbar (10^5 kPa) the elastic tensor in Voigt notation reads as

$$\underline{\underline{C}} = \begin{pmatrix} 2231 & 1165 & 1253 & 0 & -174 & 0 \\ 1165 & 3332 & 750 & 0 & 122 & 0 \\ 1253 & 750 & 3300 & 0 & 73 & 0 \\ 0 & 0 & 0 & 503 & 0 & 174 \\ -174 & 122 & 73 & 0 & 686 & 0 \\ 0 & 0 & 0 & 174 & 0 & 942 \end{pmatrix}. \quad (5)$$

It should be noted that only accidentally $C_{46} \approx -C_{15}$ holds. Indeed, they are independent elastic constants and their absolute values differ numerically by about 0.5 kbar. As a cross-check one can evaluate the bulk modulus from the relationships $9B_0 = C_{11} + C_{22} + C_{33} + 2C_{12} + 2C_{23} + 2C_{13}$ (Voigt average) or $1/B_0 = S_{11} + S_{22} + S_{33} + 2S_{12} + 2S_{23} + 2S_{13}$ (Reuss average) where S_{ij} , the tensor of elastic compliances, is the inverse of tensor C_{ij} of elastic constants. The Reuss average is expected to be closest to the value obtained from a Vinet equation of states (EOS) fit because there a uniform isotropic stress is assumed reflecting exactly what is done in the fit procedure. Accordingly, we prefer to give the Reuss average in the following. One finds a value of $B_0 = 1664$ kbar, in good agreement with the value of 1650 kbar found from the Vinet EOS fit. The small discrepancy of about 0.7% can be attributed to general uncertainties in the fit procedure as well as small Pulay stresses and numerical errors in the evaluation of the stress-strain relation. Overall, we expect an uncertainty of the same order of magnitude (about one percent) for all components of the elastic constant tensor.

In the rhombohedral case, symmetry reduces the number of independent tensor components to only six different components. One has to note that the structure of the tensor of elastic constants depends on the choice of the lattice vectors. The standard form which is usually discussed in the literature requires that the z axis is aligned parallel to the rhombohedral $\langle 111 \rangle$ direction (c axis in a hexagonal representation of the rhombohedral lattice). This can be achieved by using the lattice

vectors

$$\begin{aligned} \mathbf{a}_1 &= (0, \sqrt{3} a_{\text{hex}}/3, c_{\text{hex}}/3), \\ \mathbf{a}_2 &= (-a_{\text{hex}}/2, -\sqrt{3} a_{\text{hex}}/6, c_{\text{hex}}/3), \\ \mathbf{a}_3 &= (a_{\text{hex}}/2, -\sqrt{3} a_{\text{hex}}/6, c_{\text{hex}}/3) \end{aligned} \quad (6)$$

instead of those given in Eq. (2). For the definition of the hexagonal lattice constants a_{hex} and c_{hex} , see Sec. III B. Using these standard lattice vectors (6) we obtain in Voigt notation and units of kbar (10^5 kPa) the elastic tensor

$$\underline{\underline{C}} = \begin{pmatrix} 3815 & 1736 & 1260 & -173 & 0 & 0 \\ 1736 & 3815 & 1260 & 173 & 0 & 0 \\ 1260 & 1260 & 3458 & 0 & 0 & 0 \\ -173 & 173 & 0 & 797 & 0 & 0 \\ 0 & 0 & 0 & 0 & 797 & -173 \\ 0 & 0 & 0 & 0 & -173 & 1040 \end{pmatrix}. \quad (7)$$

The relation $C_{56} = C_{14} = -C_{24}$ is enforced by symmetry. Again, as a cross-check the bulk modulus can be calculated. One obtains $B_0 = 2157$ kbar, again very close to the value of 2150 kbar found from the Vinet EOS fit (0.3% deviation). Another excellent check is the verification that $C_{66} = (C_{11} - C_{12})/2$, enforced by symmetry and found to be fulfilled numerically exact.

The cubic bixbyite structure possesses an elastic tensor of maximum symmetry with only three independent elastic constants. In Voigt notation and units of kbar (10^5 kPa), the elastic tensor is

$$\underline{\underline{C}} = \begin{pmatrix} 3411 & 1226 & 1226 & 0 & 0 & 0 \\ 1226 & 3411 & 1226 & 0 & 0 & 0 \\ 1226 & 1226 & 3411 & 0 & 0 & 0 \\ 0 & 0 & 0 & 760 & 0 & 0 \\ 0 & 0 & 0 & 0 & 760 & 0 \\ 0 & 0 & 0 & 0 & 0 & 760 \end{pmatrix}. \quad (8)$$

The bulk modulus is found to be $B_0 = 1954$ kbar, also close to the value of 1930 kbar found from the Vinet EOS fit (1.2% deviation).

Finally, in the orthorhombic case symmetry is a bit reduced again but still rather high with nine independent elastic constants. In Voigt notation and units of kbar (10^5 kPa), the elastic tensor is

$$\underline{\underline{C}} = \begin{pmatrix} 3120 & 1544 & 1262 & 0 & 0 & 0 \\ 1544 & 2736 & 1268 & 0 & 0 & 0 \\ 1262 & 1268 & 2798 & 0 & 0 & 0 \\ 0 & 0 & 0 & 724 & 0 & 0 \\ 0 & 0 & 0 & 0 & 473 & 0 \\ 0 & 0 & 0 & 0 & 0 & 920 \end{pmatrix}. \quad (9)$$

Again, we can calculate the bulk modulus and we find a value of $B_0 = 1855$ kbar. In this case, we have not performed any Vinet EOS fit and cannot compare.

IV. BAND STRUCTURES

A. General trends: DFT-GGA results

As a preliminary study, we present band structures and densities of states of all polymorphs on pure DFT-GGA level.

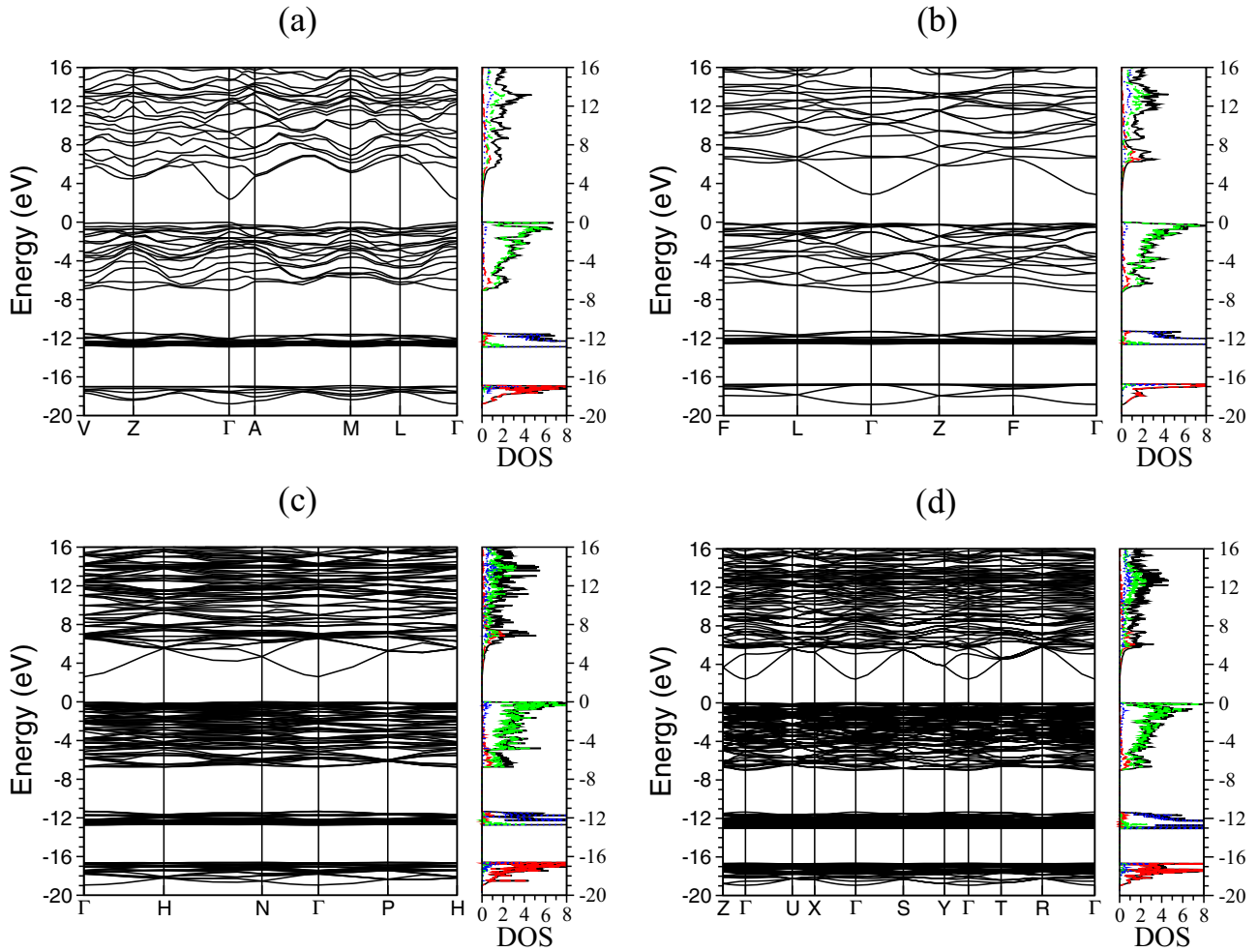


FIG. 1. Comparison of the DFT band structures of four different Ga_2O_3 polymorphs: (a) monoclinic, (b) rhombohedral, (c) cubic, and (d) orthorhombic. In addition, the total (black full line), as well as the s - (red dashed line), p - (green dotted-dashed line), and d -projected (blue dotted line) DFT DOS is displayed. The valence band maxima are all aligned to zero energy.

Although we lack quasiparticle effects on this level resulting in too small gaps (and also wrong Ga $3d$ positions), the band dispersions (and also band orderings) are widely described reasonably as well as trends in the gaps with the polymorphs. The band structures and densities of states displayed in Fig. 1 demonstrate that the energetic positions of the groups of bands (representing O $2s$, Ga $3d$, and O $2p$ in the valence band region and Ga $4s$, Ga $4p$, and Ga $4d$ in the lower part of the conduction bands) are rather similar. This is clearly reflected in the densities of states. A comparison of all densities of states shown in Fig. 2 demonstrates that the overall shapes of the DOSs are very similar (apart from slightly varying gaps and some jerkiness due to insufficient k sampling). This will still be observed later on the GW level for the monoclinic and rhombohedral phases. One may conclude that due to the strong ionic Ga-O bonding, the actual arrangement of the Ga and O atoms has a minor influence on the energy distribution of the empty and occupied electronic states.

An important question for the optical absorption properties is whether the polymorphs possess direct or indirect gaps. Independent of the polymorph, all band structures show a pronounced conduction band minimum (CBM) at the Γ

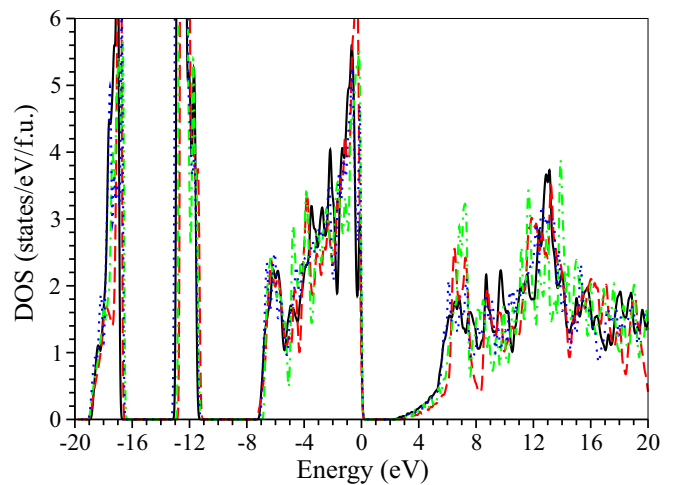


FIG. 2. Comparison of the total DFT DOS per formula unit (f.u.) of four different Ga_2O_3 polymorphs: monoclinic (black full line), rhombohedral (red dashed line), cubic (green dotted-dashed line), and orthorhombic (blue dotted line). The valence band maxima (energy zero) are used for the alignment. A Gaussian broadening of 0.1 eV is applied.

TABLE VI. Calculated DFT band structure data for all four polymorphs under consideration. All values are given in eV.

| Polymorph | Monocl. | Rhomboh. | Cubic | Orthorh. |
|------------------------|----------|----------|----------|-----------|
| Gap character | Indirect | Indirect | Indirect | Indirect? |
| Direct gap at Γ | 2.377 | 3.075 | 2.696 | 2.466 |
| Indirect gap | 2.356 | 2.832 | 2.594 | 2.465 |
| Valence band width | 18.789 | 18.880 | 18.950 | 18.943 |

point. In contrast, the uppermost O $2p$ derived valence bands are relatively flat. The exact position of the valence band maximum (VBM) therefore depends on the details of the atomic arrangements. The gap is clearly indirect for the rhombohedral corundum phase and is about 0.25 eV smaller than the direct gap at Γ with a valence band maximum off of high-symmetry lines, somewhere in the region around the F point. There is an almost direct gap in the monoclinic β phase. Although experiments seem to predict a clear indirect gap (about 0.1 eV smaller than the direct gap at Γ), we can only see a small difference of about 21 meV between the indirect gap from (approximately) M to Γ . This is in agreement with other DFT calculations [12,43]. Also, the cubic bixbyite structure exhibits an indirect gap from about three quarters of the Γ - N line to Γ which is about 0.1 eV smaller than the direct gap at Γ . An undetermined situation is found for the orthorhombic phase. It possesses a quasidirect gap although it seems that the valence band maximum is a bit off Γ in the Γ - X direction but with a small difference of only 1 meV which is of the order of the numerical error.

All direct and indirect DFT band-gap values are summarized in Table VI. In addition, also the valence band widths are listed. One can observe that there are some differences in the gap values but almost no change in the valence band widths due to the different atomic arrangements. However, overall all polymorphs display gaps of similar order of magnitude (order of 2.5 eV).

B. Quasiparticle bands

In Figs. 3 and 4, we depict the band structures calculated on GW level over a wide energy range and in a more narrow energy range close to the fundamental gap region. Compared to the DFT-GGA results presented in the previous subsection one can see a clear gap opening within the HSE+ G_0W_0 approach. Table VII summarizes some key data (direct and indirect gaps) of the two polymorphs under consideration. The gap openings within HSE+ G_0W_0 with respect to DFT-GGA amount to about 2.7 eV (2.55 eV) for the β phase (α phase), i.e., they are approximately as large as the DFT-GGA gaps of 2.36 eV (2.83 eV).

The absolute values in Table VII agree well with experimental data. For β -Ga₂O₃ recent ARPES studies [16] found a value of 4.9 eV as a lower bound for the size of the quasiparticle band gap. Optical absorption measurements [3] seem to indicate slightly lower values but for the optical gap as will be discussed below. For α -Ga₂O₃, the fundamental gap is opened by 0.3–0.6 eV. This trend agrees with optical transmittance measurements [44] which indicate an optical gap of 4.98 eV for α -Ga₂O₃, about 0.2 eV larger than the optical gap of 4.8 eV estimated for β -Ga₂O₃.

One of the most remarkable results in Fig. 4 is that for the monoclinic β phase the valence band maximum near M is now about 8 meV lower than the maximum at Γ , i.e., that on GW level the β phase appears as a direct-gap semiconductor (in contrast to DFT-GGA and also to HSE which still yields a difference of about 7 meV in favor of an indirect gap, consistent with DFT-GGA results). However, within all numerical uncertainties and error bars, this very weak direct character or quasidegeneracy between direct and indirect gaps is not conclusive. To be honest, possible error bars leave room for uncertainties of ± 0.1 eV or even more. In contrast to these findings, for the rhombohedral α phase we still clearly find an indirect gap, about 0.24 eV smaller than the direct one (close to the DFT-GGA result of 0.25 eV and the HSE result of about 0.23 eV).

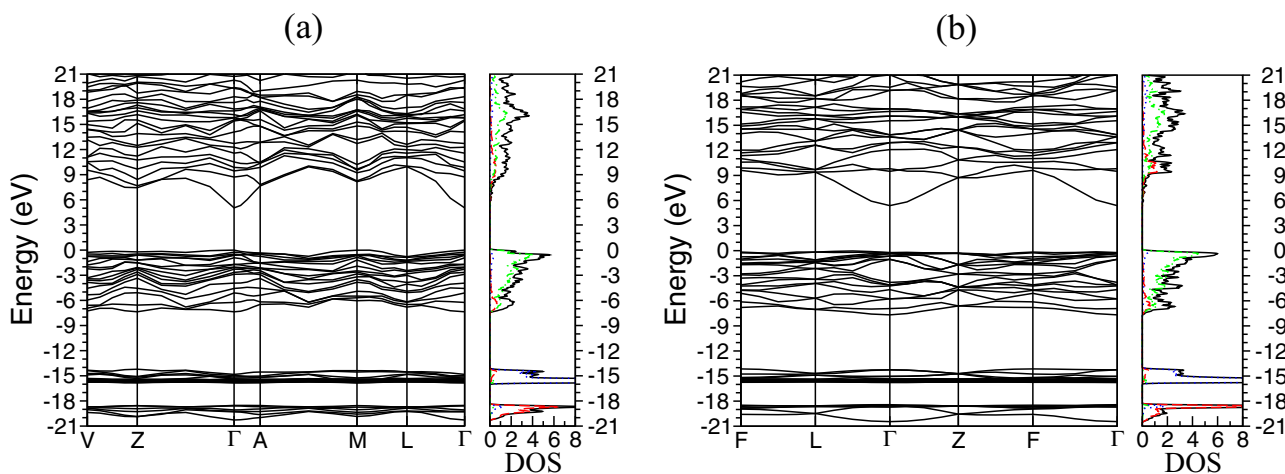


FIG. 3. Quasiparticle band structures at HSE+ G_0W_0 level of the (a) monoclinic and (b) rhombohedral Ga₂O₃ polymorphs in the full energy range. In addition, the corresponding total (black full line), as well as the s - (red dashed line), p - (green dotted-dashed line), and d -projected (blue dotted line) DOS is displayed. The valence band maxima are used as energy zero.

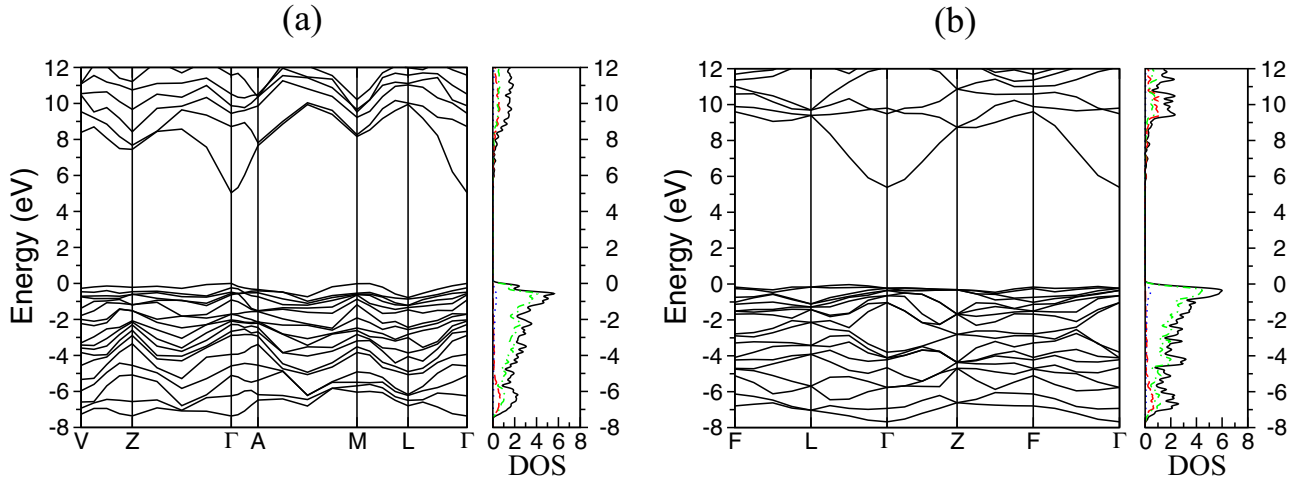


FIG. 4. Quasiparticle band structures at HSE+ G_0W_0 level of the (a) monoclinic and (b) rhombohedral Ga_2O_3 polymorphs in an energy range around the fundamental gap. In addition, the corresponding total (black full line), as well as the s - (red dashed line), p - (green dotted-dashed line), and d -projected (blue dotted line) DOS is displayed. The valence band maxima are used as energy zero.

C. Effective electron mass tensors

For the monoclinic β phase and the rhombohedral α phase, we also determine the effective mass tensor for electrons at the conduction band minimum. Due to the complex valence band structure, we shall not discuss hole masses here. The reciprocal effective electron mass tensor is defined by

$$(m_{ij}^*)^{-1} = \frac{1}{\hbar^2} \frac{\partial^2}{\partial k_i \partial k_j} E_c(\mathbf{k}) \Big|_{\mathbf{k}=0} \quad (10)$$

with $E_c(\mathbf{k})$ as the dispersion of the lowest conduction band. In order to obtain a good quadratic fit we need to sample different directions in \mathbf{k} space close to the BZ center very densely. This becomes practically impossible on the GW level due to CPU time and memory restrictions. Therefore, we restrict ourselves to calculations on the HSE level. A comparison of HSE and GW band structures (not displayed here) shows that the band dispersions of the lowest conduction band are almost identical (within few percent) so that we can consider the HSE results to be of similar quality as GW results.

Very careful fits involving 11 \mathbf{k} points (Γ and five \mathbf{k} points right and left of Γ) in different directions with a spacing of 0.002 reciprocal lattice constants yield first the inverse mass tensor. By inversion of this tensor we obtain finally the mass tensor itself. In the monoclinic case, it possesses three different diagonal elements and in addition a nonvanishing nondiagonal element m_{xz}^* if we choose the a axis to be parallel to the x axis, the b axis to be parallel to the y axis, and consequently the c axis to be in the xz plane with an angle $\beta - 90^\circ$ off

the z axis. In the rhombohedral case, we have to determine two representations: In the rhombohedral representation, all diagonal elements are identical (and correspond to the average mass) and all nondiagonal elements are nonvanishing and identical (representing the anisotropy). A more conventional and easier representation of this is the hexagonal one: Here, the matrix is diagonal and assuming the c axis to be parallel to the z axis, we obtain two identical masses $m_{xx}^* = m_{yy}^*$ (identical to the difference between the diagonal and the off-diagonal elements in rhombohedral representation) and an independent second mass m_{zz}^* (given by m_{xx}^* plus three times the off-diagonal element in rhombohedral representation).

The resulting electron effective mass tensors in units of the free electron mass m_0 are

$$\underline{\underline{m}}^* = \begin{pmatrix} 0.272 & 0.000 & 0.002 \\ 0.000 & 0.270 & 0.000 \\ 0.002 & 0.000 & 0.263 \end{pmatrix} m_0 \quad (11)$$

in the monoclinic case,

$$\underline{\underline{m}}^* = \begin{pmatrix} 0.256 & 0.003 & 0.003 \\ 0.003 & 0.256 & 0.003 \\ 0.003 & 0.003 & 0.256 \end{pmatrix} m_0 \quad (12)$$

in the rhombohedral case (rhombohedral representation), or

$$\underline{\underline{m}}^* = \begin{pmatrix} 0.253 & 0.000 & 0.000 \\ 0.000 & 0.253 & 0.000 \\ 0.000 & 0.000 & 0.262 \end{pmatrix} m_0 \quad (13)$$

if we chose the hexagonal representation for the rhombohedral phase.

As one can see, the anisotropies are rather small (maximum about 3.5%) and the masses also do not vary too much with the polymorph (the rhombohedral masses are just about 4% smaller than the monoclinic ones). The average masses of $0.268 m_0$ ($0.256 m_0$) for the monoclinic (rhombohedral) phase match also quite well a recent estimate of Varley *et al.* [43] who found a value of $0.28 m_0$ in the monoclinic case and a

TABLE VII. Summary of quasiparticle gap data for the monoclinic and rhombohedral polymorphs. All values are given in eV.

| Polymorph | Monoclinic | Rhombohedral |
|------------------------|----------------|--------------|
| Gap character | “Undetermined” | Indirect |
| Direct gap at Γ | 5.038 | 5.625 |
| Indirect gap | 5.046 | 5.387 |

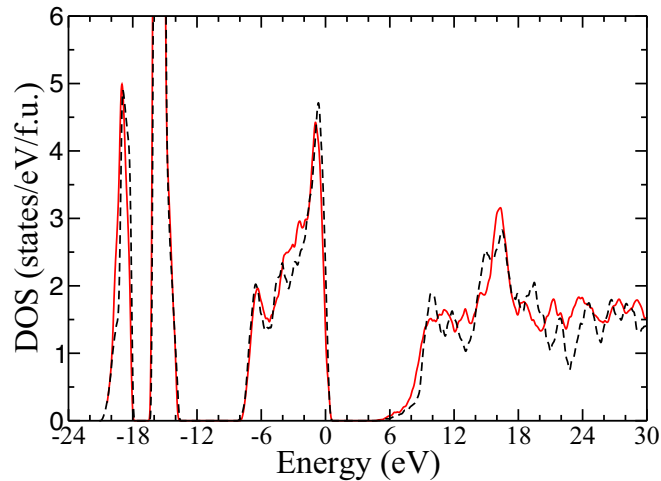


FIG. 5. Comparison of the total quasiparticle DOS at HSE+ G_0W_0 level of the monoclinic (red full line) and rhombohedral (black dashed line) Ga₂O₃ polymorphs. The valence band maxima (energy zero) are used for the alignment. A Gaussian broadening of 0.1 eV is applied.

very crude experimental estimate [45] which claims a value of about $0.3 m_0$.

D. Density of states

Also, apart from the larger gap of the rhombohedral phase, the DOSs look again very similar as in the DFT-GGA case, as demonstrated in Fig. 5. The most significant differences occur in the lower-energy regions of the conduction bands. So, implicitly we can speculate that this might also hold for the other polymorphs (if we could afford a GW calculation). It is also important to note that, as it can already be observed at DFT level, there is a clearly visible hybridization between the Ga $3d$ and the O $2s$ states in the l -projected DOS for all polymorphs under consideration. A detailed analysis (site- and l -projected DOS) displayed in Fig. 6 for the monoclinic polymorph at the GW level demonstrates that there is in addition hybridization between Ga $4s$ and O $2p$ states in the lower part of the topmost group of mostly O $2p$ related valence bands. But, even to some extent a Ga $4p$ character of the states is found in the center of this band group and finally some small Ga $3d$ character is found close to the top of the valence bands. This holds again for all polymorphs already on DFT level (not shown here). It is remarkable that exactly the same behavior has been found for In₂O₃ [46]. Since the energetic positions of In $4d$ and O $2s$ in In₂O₃ are not too different from those of Ga $3d$ and O $2s$ in Ga₂O₃, this result is not surprising because we can expect similar interactions between these states.

Recent experimental work [47] seems to confirm this result. However, it seems that the Ga $3d$ binding energy is a bit underestimated (by about 1 eV) in the calculation. It cannot be excluded that we suffer similar convergence problems for the strongly localized d levels as reported for the case of ZnO [48]. The consequence seems to be an underestimation of the O $2s$ –Ga $3d$ hybridization. For more details, we point the reader to Ref. [47] where our calculated l -projected DOS and corresponding band structure in the valence band region

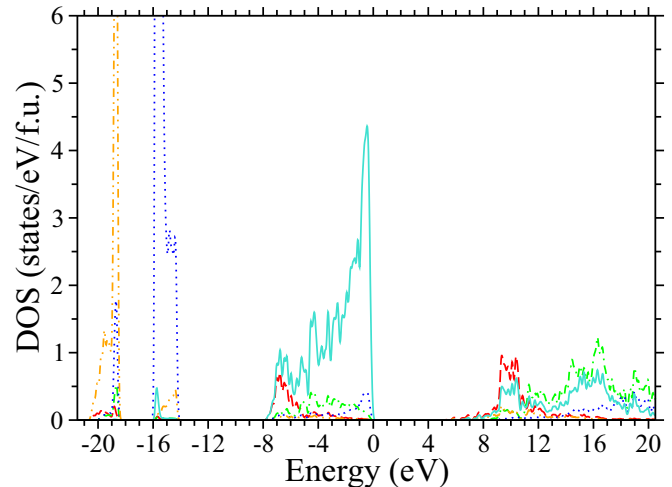


FIG. 6. Site- and l -projected DOS at HSE+ G_0W_0 level for the monoclinic Ga₂O₃ polymorph: Ga $4s$ (red dashed line), Ga $4p$ (green dotted-dashed line), Ga $3d$ (blue dotted line), O $2s$ (orange dotted-dotted-dashed line), and O $2p$ (turquoise full line). The valence band maximum is used as energy zero. A Gaussian broadening of 0.1 eV is applied.

of β -Ga₂O₃ has already been published previously along with core-level photoelectron spectra and a discussion of the hybridization effects. However, a binding energy of Ga $3d$ electrons of about 15.7 eV [12] is difficult to derive from an x-ray photoemission spectrum (XPS) of a TCO [49] because of the electrons in the CBM. Its reference to the VBM asks for the knowledge of the gap. Nevertheless, the main Ga $3d$ derived peak in Fig. 6 occurring at about 15.5 eV binding energy is close to such a binding energy.

V. DIELECTRIC FUNCTION

A. Symmetry and tensor character

The frequency-dependent dielectric function is not a simple scalar but a symmetric tensor of rank two, i.e., it consists in the most general case of six components ϵ_{xx} , ϵ_{yy} , ϵ_{zz} , ϵ_{xy} , ϵ_{yz} , and ϵ_{xz} . Instead of displaying these six components, one could as well diagonalize the tensor for each frequency and display the three eigenvalues plus the orientations of the three frequency-dependent optical axes (eigenvectors). However, we prefer to display here just all independent components ϵ_{ij} of the tensor. Symmetry reduces the number of independent components of the tensor ϵ_{ij} to a maximum of four [50].

In the simple case of cubic crystals, for example, the tensor takes a form proportional to the unit tensor, i.e., one component (e.g., ϵ_{xx}) is sufficient to characterize the dielectric tensor. In the case of hexagonal, but also rhombohedral, structures one obtains two independent components. In the hexagonal case, the tensor is diagonal if we assume that the hexagonal c axis is parallel to the Cartesian z axis. In this case, it holds $\epsilon_{xx} = \epsilon_{yy} \neq \epsilon_{zz}$ and all other components vanish, i.e., ϵ_{xx} and ϵ_{zz} are sufficient to characterize the dielectric tensor. In the rhombohedral case, one finds instead $\epsilon_{xx} = \epsilon_{yy} = \epsilon_{zz}$ but nonzero nondiagonal elements $\epsilon_{xy} = \epsilon_{yz} = \epsilon_{xz}$. One of the diagonal and one of the nondiagonal

elements (ϵ_{diag} and $\epsilon_{\text{nondiag}}$) will then characterize the dielectric tensor. Many people may prefer a hexagonal representation of the rhombohedral lattice and like to express the dielectric tensor in terms of some $\epsilon_{xx,h}$ and $\epsilon_{zz,h}$. This is easily achieved by the transformations $\epsilon_{xx,h} = \epsilon_{\text{diag}} - \epsilon_{\text{nondiag}}$ and $\epsilon_{zz,h} = \epsilon_{\text{diag}} + 2\epsilon_{\text{nondiag}}$. By these transformations it becomes, by the way, obvious that ϵ_{diag} itself provides the isotropically averaged dielectric function and that $3\epsilon_{\text{nondiag}}$ gives the resulting anisotropy $\epsilon_{zz,h} - \epsilon_{xx,h}$.

In the orthorhombic case with Cartesian axis aligned to the three crystal axes, one obtains also a simple form with three independent diagonal components $\epsilon_{xx} \neq \epsilon_{yy} \neq \epsilon_{zz}$ which are sufficient to characterize the dielectric tensor. More complicated is the monoclinic system which has to be handled in the case of $\beta\text{-Ga}_2\text{O}_3$. Here, four independent tensor elements occur and the structure of the tensor depends on the choice of the Cartesian axis with respect to the crystal lattice vectors. In our case, we have chosen the Cartesian x axis to be aligned with the monoclinic a axis and the y axis to be aligned with the monoclinic b axis (which is orthogonal to both the a and the c axes). This means the monoclinic c axis is somewhat off the Cartesian z axis and lies inside the Cartesian xz plane. This setup results in $\epsilon_{xy} = \epsilon_{yz} = 0$. All other four remaining components (ϵ_{xx} , ϵ_{yy} , ϵ_{zz} , and ϵ_{xz}) are nonvanishing and different. These four components are displayed in the following figures for the monoclinic Ga_2O_3 polymorph.

B. Independent-particle spectra

As in the case of band structures and densities of states, we also present a preliminary study on the independent-particle level for all polymorphs. The components of the frequency-dependent dielectric tensor are computed by means of the DFT-GGA Kohn-Sham eigenenergies and eigenfunctions. As we will demonstrate in the next subsections many-body effects, such as quasiparticle and excitonic effects, significantly influence optical spectra.

The DFT-GGA spectra are displayed in Fig. 7 for the four Ga_2O_3 polymorphs under consideration. Apart from the off-diagonal elements of the dielectric tensor in the monoclinic and rhombohedral cases, the diagonal elements, their real and imaginary parts, are rather similar. This holds especially for the real parts. For vanishing frequency, the static electronic dielectric constants $\epsilon_{jj}^\infty = \text{Re}\epsilon_{jj}(\omega = 0) \approx \bar{\epsilon}^\infty$ are rather independent of the polarization direction j and the polymorph. Within the random-phase approximation, i.e., the DFT-GGA, it holds $\bar{\epsilon}^\infty = 4.12$ (monoclinic), $\bar{\epsilon}^\infty = 4.38$ (rhombohedral), $\bar{\epsilon}^\infty = 4.28$ (cubic), and $\bar{\epsilon}^\infty = 4.26$ (orthorhombic). Also the zeros, $\text{Re}\epsilon_{jj} = 0$, appear in the same energy region $\hbar\omega = 14.6 - 16.6$ eV.

The strongest variations with the polymorph happen in the range of the optical interband transitions as especially indicated by the imaginary parts. However, the principal frequency dependence is similar as a consequence of the weakly varying joint density of states, which follows the single-particle densities of states in Fig. 2. The spectral variations are mainly due to slightly modified van Hove singularities in the band structures in Fig. 1. The variations in the intensities are considerably related to the optical transition matrix elements. This is underlined by the averaged

dielectric functions $\bar{\epsilon}(\omega) = \frac{1}{3} \sum_{j=1}^3 \epsilon_{jj}(\omega)$ displayed in Fig. 8. Their variation with the polymorph mainly occurs in the photon energy range $\hbar\omega = 5 - 10$ eV. The dielectric function of $\alpha\text{-Ga}_2\text{O}_3$ is the largest, whereas that of $\beta\text{-Ga}_2\text{O}_3$ is the smallest. This fact expresses the (global) oscillator-strength sum rule which yields the plasmon frequency square and, hence, a value $\propto V_0^{-1}$ [21]. Indeed, the spectra in the energy range of 5–10 eV follow the volumes V_0 in Table I.

C. Global excitonic spectra

Figures 9 and 10 display the excitonic spectra of the stable $\beta\text{-Ga}_2\text{O}_3$ and the metastable $\alpha\text{-Ga}_2\text{O}_3$ polymorph. Also, for comparison spectra in independent-quasiparticle approximation [51] at GW level (including local-field effects) are shown in Figs. 9 and 10. In addition, as in the DFT-GGA case, we also compare the averaged dielectric functions of the two polymorphs under consideration. This is displayed in Fig. 11 (again at GW and BSE levels). While the HSE+ G_0W_0 spectra are more or less blue-shifted variations of the DFT-GGA spectra, there is a significant redistribution of oscillator strength from higher to lower photon energies in the BSE spectra. Some additional features become visible for transition energies below the fundamental gap energy. These features are related to bound exciton states [21]. Figure 12 displays the imaginary part of the dielectric function in the onset region around the fundamental gap energy, i.e., the absorption edge, in more detail.

Several interesting features can be observed in Figs. 9–12. Two general features of the excitonic effects are obvious. The imaginary parts near the absorption edge and in the range of the interband transitions are increased. The same trend is visible for the real parts as a consequence of the oscillator-strength and screening sum rules. The inclusion of excitonic effects also enhances the differences between the averaged dielectric functions of both polymorphs, which are still rather weak in the GW case (as they are in the DFT case). This holds in particular for the lower-energy range (below about 13 eV). Surprisingly, despite the low symmetry of both polymorphs, the anisotropies remain rather moderate to weak. They are just a bit more pronounced in the energy region of the main interband transitions. Excitonic effects enhance the anisotropies but still not in a dramatic way. Very significant anisotropies can, however, be observed in the onset region close to the fundamental gap energy. There, the crystal-field splittings of the O $2p$ valence band states become visible in conjunction with their orbital character (mostly p_x/p_y -like or mostly p_z -like) and different selection rules for different light polarization. Although we have no pure p_x/p_z states due to the monoclinic angle different from 90° the character is still mostly p_x/p_z -like. So, there are no absolutely strict selection rules, but at least something what one could call dominating selection rules that give rise to a clear polarization dependence of the lowest transitions from O $2p$ valence to Ga $4s$ conduction band states. From that point of view, one has also to interpret the excitonic peaks visible in Fig. 12. In any case, the visible excitonic peaks below the (direct) HSE+ G_0W_0 quasiparticle gaps $E_g = 5.04$ eV (monoclinic) and $E_g = 5.63$ eV (rhombohedral) indicate bound electron-hole pairs. The position of the absorption edge with excitonic effects is

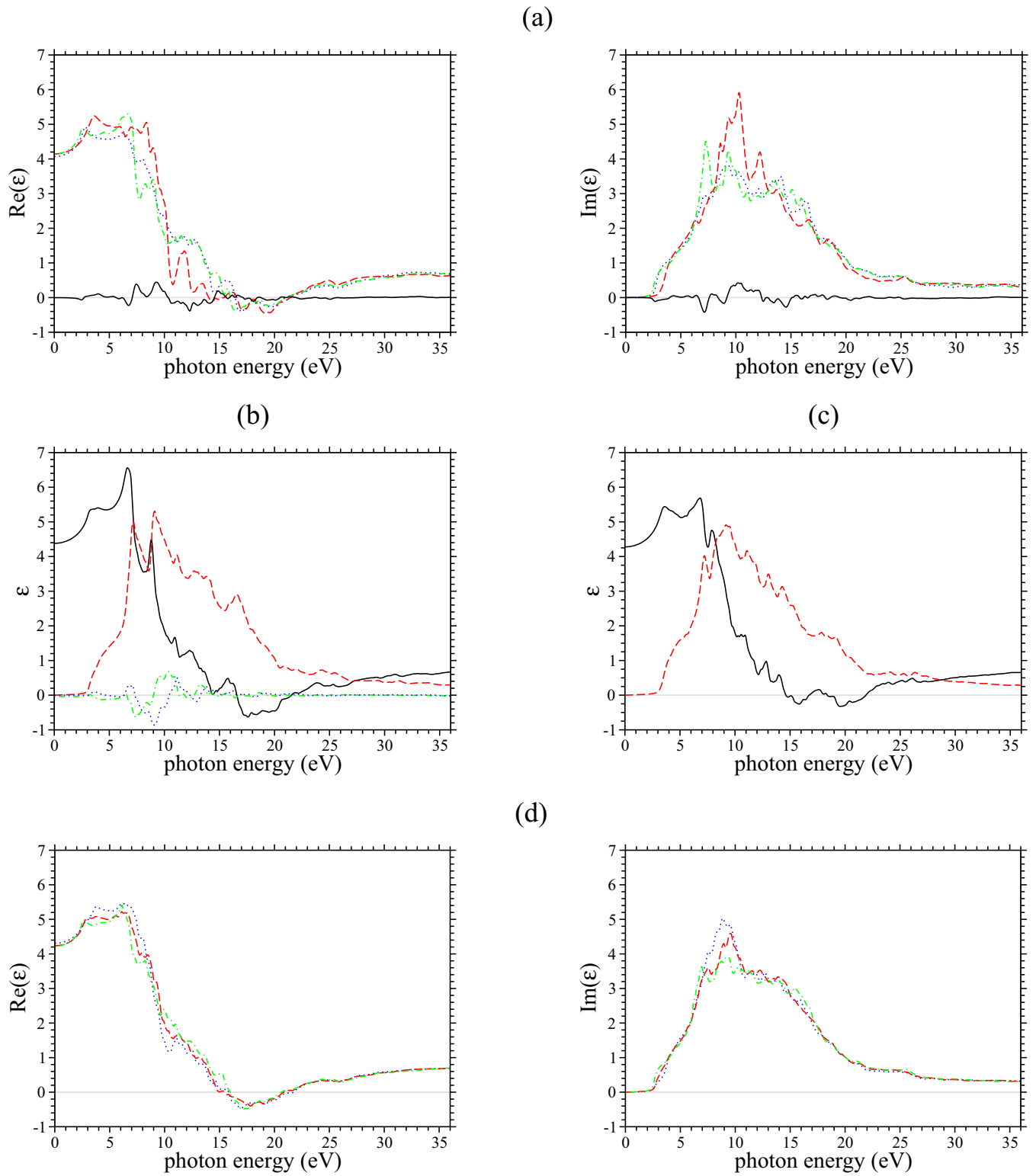


FIG. 7. Dielectric function of the (a) monoclinic, (b) rhombohedral, (c) cubic, and (d) orthorhombic Ga₂O₃ polymorphs at DFT level. For the monoclinic and the orthorhombic cases, the left panels show the real part and the right panels the imaginary part with components xx (blue dotted line), yy (red dashed line), zz (green dotted-dashed line), and (monoclinic case only) xz (black full line). For the rhombohedral and the cubic cases, real and imaginary parts are displayed simultaneously with the components $xx = yy = zz$ (black full line for real part, red dashed line for imaginary part) and (rhombohedral case only) $xy = yz = xz$ (green dotted-dashed line for real part and blue dotted line for imaginary part).

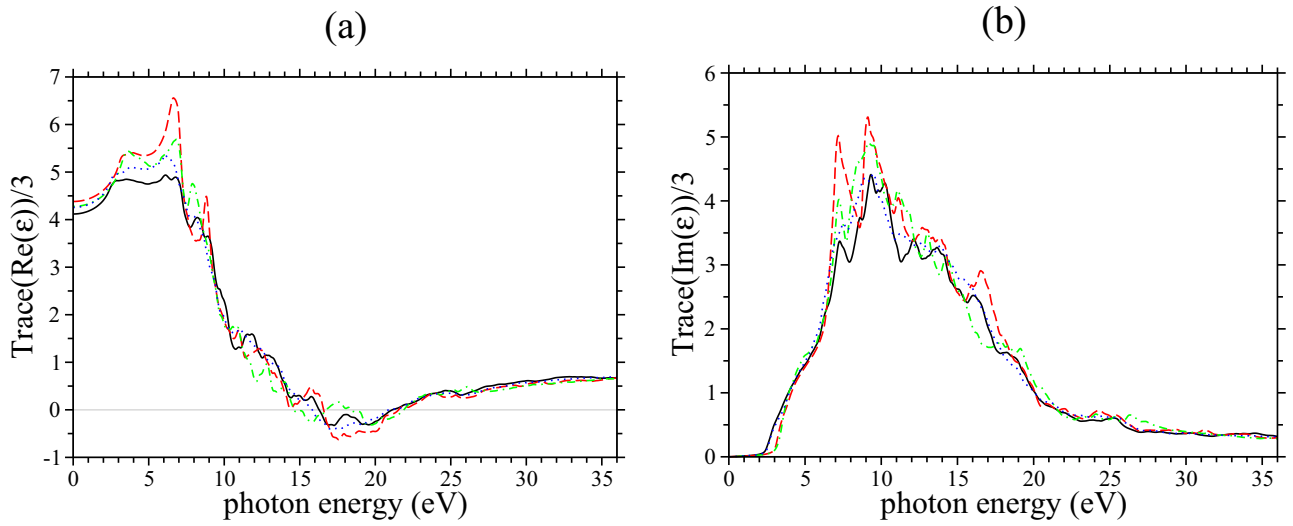


FIG. 8. Comparison of the isotropically averaged dielectric function [(a) real part, (b) imaginary part] at DFT level of four different Ga_2O_3 polymorphs: monoclinic (black full line), rhombohedral (red dashed line), cubic (green dotted-dashed line), and orthorhombic (blue dotted line).

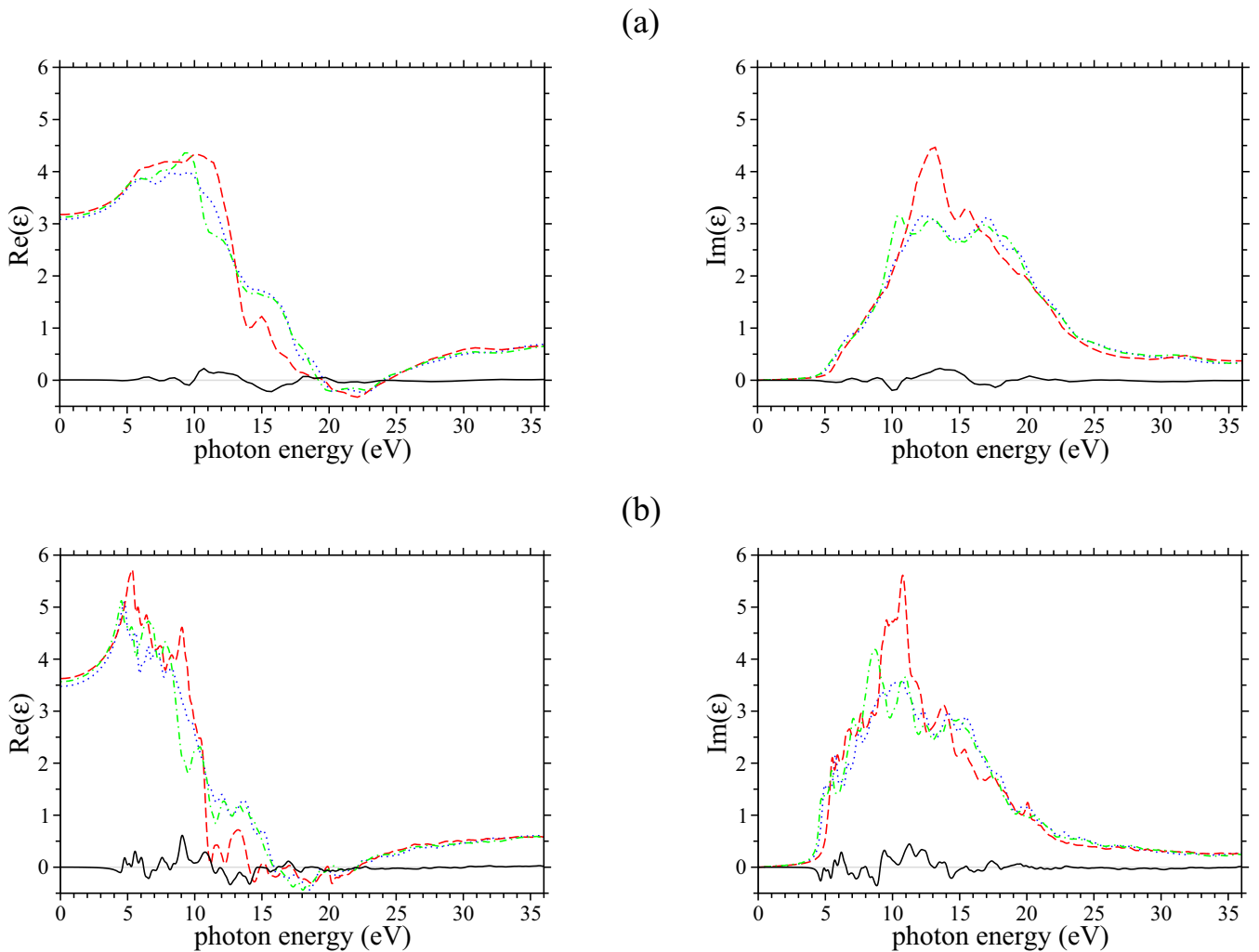


FIG. 9. Dielectric function (left real part, right imaginary part) of the monoclinic $\beta\text{-Ga}_2\text{O}_3$ polymorph at (a) HSE+ G_0W_0 and (b) BSE level. The four independent components are displayed: xx (blue dotted line), yy (red dashed line), zz (green dotted-dashed line), and xz (black full line).

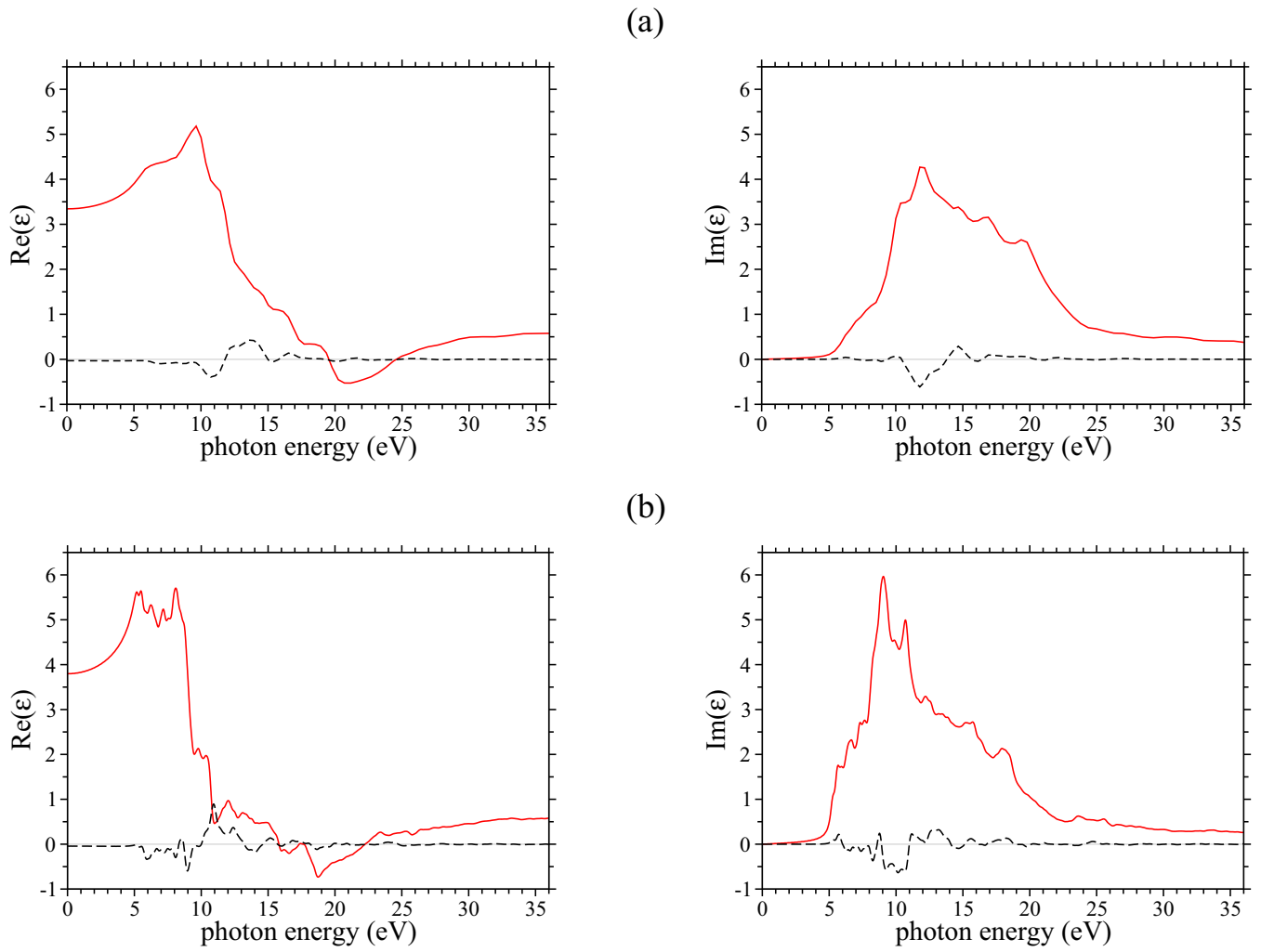


FIG. 10. Dielectric function (left panels real part, right panels imaginary part) of the rhombohedral α -Ga₂O₃ polymorph at (a) HSE+ G_0W_0 and (b) BSE level. A rhombohedral representation is used with the diagonal elements $xx = yy = zz$ (red full line) and $xy = yz = xz$ (black dashed line) (see Sec. V A).

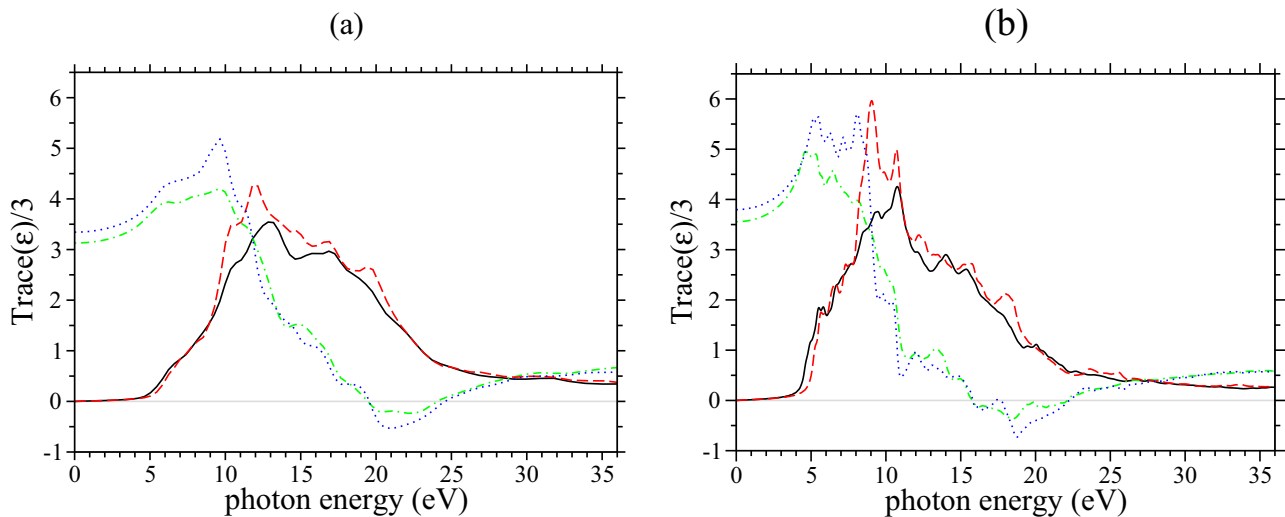


FIG. 11. Comparison of isotropically averaged dielectric function of monoclinic and rhombohedral Ga₂O₃ polymorphs at (a) HSE+ G_0W_0 and (b) BSE levels: monoclinic real part (green dotted-dashed line), monoclinic imaginary part (black full line), rhombohedral real part (blue dotted line), and rhombohedral imaginary part (red dashed line).

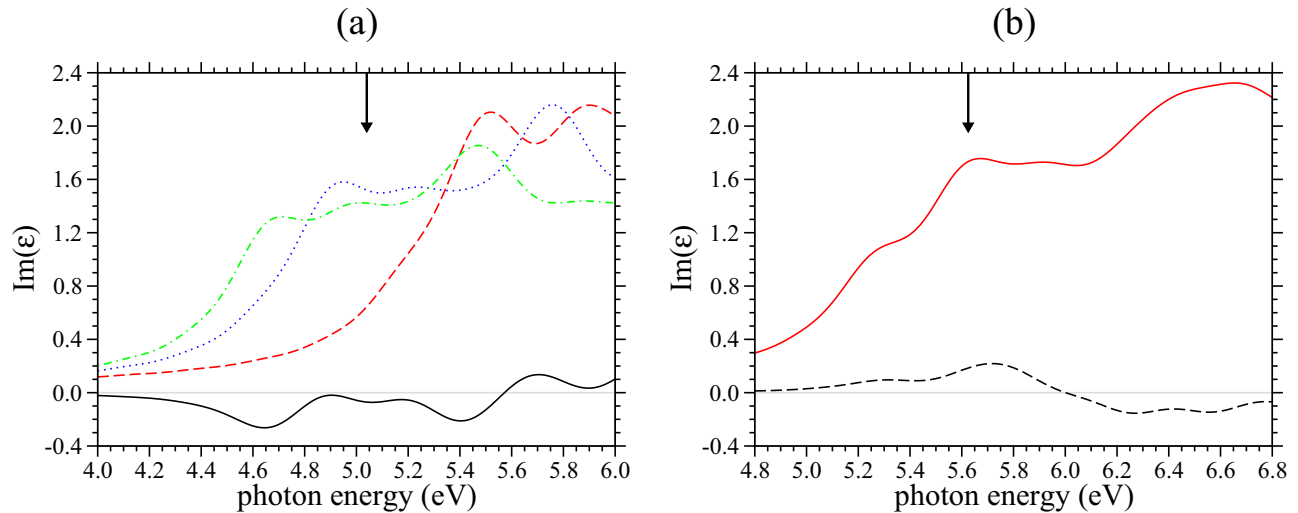


FIG. 12. Imaginary part of dielectric function of (a) monoclinic and (b) rhombohedral Ga_2O_3 polymorphs at BSE level. The components are xx (blue dotted line), yy (red dashed line), zz (green dotted-dashed line), and xz (black full line) in the monoclinic case and $xx = yy = zz$ (red full line) and $xy = yz = xz$ (black dashed line) in the rhombohedral case. The position of the direct HSE+ G_0W_0 quasiparticle gap at Γ is indicated by a vertical arrow.

much lower in energy in the monoclinic case (at least for x or z light polarization) compared to the rhombohedral case. These facts explain the different edges observed in absorption and transmittance measurements [3,14,44,52].

D. Absorption edges

Since the effective optical gap, i.e., onset of strongly allowed optical transitions is different for different polarizations one has to expect that the same holds also for the excitonic gaps. In principle, one should find different binding energies related to different interband transitions for different polarizations. In Fig. 12, it seems that the excitonic onsets follow the differences in the splittings of the valence p states. Since the time-evolution method [28] used to determine the excitonic spectra does not give access to the excitonic eigenvalues and eigenfunctions, we cannot really prove which valence $O\ 2p$ states are coupled to which conduction $\text{Ga}\ 4s$ states. But, we can at least analyze the lowest quasiparticle interband transition energies on GW level. In the onset region, only transitions from the topmost group of mostly $O\ 2p$ related valence bands into the lowest $\text{Ga}\ 4s$ related conduction band can occur and will contribute significantly to the excitonic transitions. Some transitions are very weak or almost forbidden, some of them are very strong and should explain the observable peaks. It should be noted that transitions from these states into the second-lowest conduction band at Γ behave exactly complementary because of the different nodal structure of the (still $\text{Ga}\ 4s$ like) wave function enforced by orthogonality to the lowest conduction band, resulting in complementary spatial overlaps with the $O\ 2p$ related valence band states. Strong or weak spatial overlaps finally determine the strengths of the interband transitions while the p_x , p_y , and p_z character of the valence band states determines the strengths of the interband transitions for different light polarization.

In order to discuss the selection rules, the monoclinic $\beta\text{-Ga}_2\text{O}_3$ is investigated in detail. Table VIII lists all transition

energies in the onset region lower than 6.5 eV at GW level and gives the orbital character (in terms of $p_x/p_y/p_z$) of the corresponding $O\ 2p$ states (which is important for the selection rules for different light polarizations) along with the transition strength and an attempt to relate this to the observed peaks of the imaginary part of the dielectric function in the onset region. From the interband transition energies in Table VIII and the exciton peak positions in Fig. 12, we conclude that the exciton binding energies of the lowest excitons (the exciton ground state) are about 0.4 eV for the $s\text{-}p_x$ and $s\text{-}p_z$ excitons but only about 0.1 eV for the $s\text{-}p_y$ excitons. One should, however, note that the assignment in the case of the $p_y \rightarrow s$ transitions is less clear from that point of view that with a very close look at ϵ_{yy} there might be an almost invisible shoulder around 5.1 eV in Fig. 12(a). If this shoulder could be assigned to the 5.6-eV interband transition (and the 6-eV interband transition to the excitonic peak at 5.5 eV, the 5.9-eV peak might then result from a 6.75-eV interband transition not listed above) the exciton binding energy could be as well about 0.5 eV for the lowest $s\text{-}p_y$ excitons. Unfortunately, the spectral resolution is not yet good enough to finally decide which is the right interpretation. Even the energetic distance of the first two peaks would be

TABLE VIII. Transition energies in eV at the Γ point at GW level for the monoclinic polymorph of Ga_2O_3 along with their orbital character and selection rules. An assignment to excitonic transition is provided as well.

| Energy | Character | Strength | Excitonic peak |
|--------|-----------------|-----------|---|
| 5.04 | Mainly p_z | Strong | ≈ 4.65 (ϵ_{zz}) |
| 5.29 | Mainly p_x | Strong | ≈ 4.90 (ϵ_{xx}) |
| 5.54 | Mixed p_x/p_z | Very weak | $\approx 5.0\text{--}5.2$ ($\epsilon_{xx}/\epsilon_{zz}$) |
| 5.62 | p_y | Strong | ≈ 5.50 (ϵ_{yy}) |
| 5.69 | p_y | Very weak | |
| 5.99 | p_y | Strong | ≈ 5.90 (ϵ_{yy}) |

the same with 0.4 eV. Only the results for the s - p_x and s - p_z excitons seem doubtless. Anyway, due to the still rather coarse \mathbf{k} mesh it should also be noted that an error bar of about 0.1–0.2 eV, at least on the scale of excitation energies, has to be taken into consideration.

More precise computations of the exciton binding energies [53] are prohibited because of CPU time requirements. Moreover, in this case also polaron effects have to be discussed, despite the fact that their influence on the quasiparticle transition energy and the exciton binding energy tend to compensate each other [54]. Nevertheless, the order of magnitude of binding energies is confirmed within a Wannier-Mott picture [21]. The calculated average conduction band mass in Sec. IV C of $m^* \approx 0.27 m_0$ dominates the reduced interband mass. Together with an average static electronic dielectric constant of $\bar{\epsilon}^\infty \approx 3.55$ (see below) an exciton binding energy of about 0.3 eV is obtained in the range of the discussed values.

Also, in the rhombohedral case an assignment of GW transition energies at the Γ point is not easy. In Fig. 12(b), there are four different transitions at Γ with GW transition energies (strengths) 5.63 eV (strong), 5.75 eV (weak), 6.04 eV (weak), and 6.43 eV (strong) in the energy region below 7 eV. If we assign the shoulder at about 5.25 eV in the BSE spectra to the lowest transition, then we would again find an exciton binding energy of about 0.4 eV as in the monoclinic case (assuming it is a Γ exciton). The remaining peaks are hard to assign. The structures at about 5.65, 5.75–5.85, and 6.65 eV in the BSE spectra might result from transitions (excitons) at \mathbf{k} points off the BZ center where the weak transitions at Γ become clearly much stronger but with increased transition energies due to the strong dispersion of the lowest conduction band. Which of the structures could result from the strong transition at 6.43-eV GW transition energy at Γ is also not clear.

E. Static dielectric constants

The averaged static electronic dielectric constants $\bar{\epsilon}^\infty = \frac{1}{3} \text{Tr} \epsilon_{jj}(\omega = 0)$ of β - and α -Ga₂O₃ are clearly visible in Fig. 11(b). The tensor character of static electronic dielectric tensor ϵ_{ij}^∞ is indicated in the left panels of Figs. 9 and 10. For β -Ga₂O₃ the off-diagonal element of the dielectric tensor nearly vanishes for $\omega \rightarrow 0$. Since both quasiparticle effects as well as electron-hole attraction and electron-hole exchange, i.e., optical local-field effects, are taken into account, we also like to compare the calculated static electronic dielectric constants ϵ_∞ with known experimental values. The calculated (isotropically averaged) value of 3.55 (3.80) for β -Ga₂O₃ (α -Ga₂O₃) matches very well the range of experimental values of 3.4–3.6 [55–57] (3.7–3.8) [58]. But not only $\bar{\epsilon}^\infty$ matches quite well. For β -Ga₂O₃, an experimentally determined frequency-dependent dielectric tensor in the energy range of 0.5–8.5 eV has already been published along with our results in the same energy range in a previous paper [59]. It should be noted by the way that these experimental results are the first successful attempt to obtain the full dielectric tensor at least in a limited spectral range. Previously, at the best isotropically averaged spectra in a rather limited spectral range could be obtained due to the lack of good single-crystalline samples. A measurement of the full dielectric tensor

for an extended spectral range of up to 30–40 eV is still missing at all. In addition, corresponding experiments for α -Ga₂O₃ are also missing so far. The experimental results shown in Ref. [59] turn out to match our results rather well, confirming the high quality and predictive power of our GW +BSE calculations for the dielectric tensor. The published dielectric constants without excitonic effects and G_0W_0 shifts in Ref. [12] significantly underestimate the values, indicating again the need for inclusion of the many-body effects.

VI. SUMMARY AND CONCLUSIONS

We presented a detailed study on the structural, elastic, electronic, and optical properties of four different Ga₂O₃ polymorphs. This study represents the first high-quality prediction of the full frequency-dependent dielectric tensor which was so far completely unknown (α -Ga₂O₃) or only partially known (β -Ga₂O₃) due to a lack of experiments on high-quality single crystals. The two most important polymorphs β -Ga₂O₃ and α -Ga₂O₃ were treated on an elaborate level using Hedin's GW approach for band structures and the Bethe-Salpeter equation for optical spectra. The other two phases were treated on DFT level only. The four polymorphs α -, β -, δ -, and ϵ -Ga₂O₃ exhibit a correlation between atomic density and energetic stability. Within the total-energy calculations, the monoclinic β phase is the most stable one with a relatively low stiffness. We showed that polymorphs underlie also pressure-induced phase transitions at zero temperature. The so far unknown full tensors of elastic constants were predicted as well.

We could show that the electronic properties of the polymorphs are quite similar (in particular the densities of states) independent of the quite different space-group symmetries on both DFT and GW level. This can be traced back to the fact that polymorphism of Ga₂O₃ arises just from different arrangements of tetrahedrally and octahedrally coordinated Ga atoms, while the bonding of the O atoms to the Ga neighbors is almost the same. Only details of the electronic structure such as band gaps and precise position and character of van Hove singularities are influenced by the actual atomic arrangement. Rather similar direct and indirect gaps have been derived for the monoclinic phase, whereas the indirect gap character of the rhombohedral polymorph is found independent of the treatment of exchange and correlation. As a consequence of the similar bonding, the isotropically averaged dielectric functions of the different polymorphs turned out to be quite similar, in particular on independent-particle DFT and independent-quasiparticle GW levels. Nevertheless, the crystal structure determines the number of independent components of the frequency-dependent dielectric tensor. The inclusion of excitonic effects on BSE level gives more pronounced differences in the region of the main absorption peaks (up to about 13–15 eV photon energy). They determine the fine structure of the absorption edge of a polymorph. We provided a detailed analysis of all (also nondiagonal) elements of the dielectric tensor. We suggested an exciton binding energy of about 0.4 eV, which, however, varies with the light polarization because of the most contributing dipole-allowed interband transitions. Calculated static electronic dielectric constants match rather well-known experimental values.

- [1] N. Ueda, H. Hosono, R. Waseda, and H. Kawazoe, *Appl. Phys. Lett.* **70**, 3561 (1997).
- [2] K. Matsuzaki, H. Yanagi, T. Kamiya, H. Hiramatsu, K. Nomura, M. Hirano, and H. Hosono, *Appl. Phys. Lett.* **88**, 092106 (2006).
- [3] N. Ueda, H. Hosono, R. Waseda, and H. Kawazoe, *Appl. Phys. Lett.* **71**, 933 (1997).
- [4] M. Higashiwaki, K. Sasaki, A. Kuramata, T. Masui, and S. Yamakoshi, *Appl. Phys. Lett.* **100**, 013504 (2012).
- [5] K. Nomura, H. Ohta, A. Tagaki, T. Kamiya, M. Hirano, and H. Hosono, *Nature (London)* **432**, 488 (2004).
- [6] F. K. Shan, G. X. Liu, W. J. Lee, G. H. Lee, I. S. Kim, and B. C. Shin, *J. Appl. Phys.* **98**, 023504 (2005).
- [7] R. Roy, V. G. Hill, and E. F. Osborn, *J. Am. Chem. Soc.* **74**, 719 (1952).
- [8] H. Yusa, T. Tsuchiya, N. Sata, and Y. Ohishi, *Phys. Rev. B* **77**, 064107 (2008).
- [9] S. Yoshioka, H. Hayashi, A. Kuwabara, F. Oba, K. Matsunaga, and I. Tanaka, *J. Phys.: Condens. Matter* **19**, 346211 (2007).
- [10] A. D. Becke, *J. Chem. Phys.* **98**, 5648 (1993); C. Lee, W. Yang, and R. G. Parr, *Phys. Rev. B* **37**, 785 (1988).
- [11] H. He, M. A. Blanco, and R. Pandey, *Appl. Phys. Lett.* **88**, 261904 (2006).
- [12] H. He, R. Orlando, M. A. Blanco, R. Pandey, E. Amzallag, I. Baraille, and M. Rérat, *Phys. Rev. B* **74**, 195123 (2006).
- [13] F. Litimein, D. Rached, R. Khenata, and H. Baltache, *J. Alloys Compd.* **488**, 148 (2009).
- [14] M. Orita, H. Ohta, M. Hirano, and H. Hosono, *Appl. Phys. Lett.* **77**, 4166 (2000).
- [15] K. Shimamura, E. G. Villora, T. Ujiie, and K. Aoki, *Appl. Phys. Lett.* **92**, 201914 (2008).
- [16] M. Mohamed, C. Janowitz, I. Unger, R. Manzke, Z. Galazka, R. Uecker, R. Fornari, J. R. Weber, J. B. Varley, and C. G. van de Walle, *Appl. Phys. Lett.* **97**, 211903 (2010).
- [17] C. Janowitz, V. Scherer, M. Mohamed, A. Krapf, H. Dwelk, R. Manzke, Z. Galazka, R. Uecker, K. Irmscher, R. Fornari, M. Michling, D. Schmeißer, J. Weber, J. B. Varley, and C. G. van de Walle, *New J. Phys.* **13**, 085014 (2011).
- [18] J. B. Varley and A. Schleife, *Semicond. Sci. Technol.* **30**, 024010 (2015).
- [19] L. Hedin, *Phys. Rev.* **139**, A796 (1965).
- [20] G. Onida, L. Reining, and A. Rubio, *Rev. Mod. Phys.* **74**, 601 (2002).
- [21] F. Bechstedt, *Many-Body Approach to Electronic Excitations: Concepts and Applications*, Springer Series in Solid-State Sciences, Vol. 181 (Springer, Berlin, 2015).
- [22] G. Kresse and J. Furthmüller, *Comput. Mater. Sci.* **6**, 15 (1996); *Phys. Rev. B* **54**, 11169 (1996).
- [23] R. Armiento and A. E. Mattsson, *Phys. Rev. B* **72**, 085108 (2005).
- [24] L. C. de Carvalho, A. Schleife, and F. Bechstedt, *Phys. Rev. B* **84**, 195105 (2011).
- [25] J. Heyd, G. E. Scuseria, and M. Ernzerhof, *J. Chem. Phys.* **118**, 8207 (2003); **124**, 219906 (2006).
- [26] F. Fuchs, J. Furthmüller, F. Bechstedt, M. Shishkin, and G. Kresse, *Phys. Rev. B* **76**, 115109 (2007).
- [27] C. Rödl, F. Fuchs, J. Furthmüller, and F. Bechstedt, *Phys. Rev. B* **77**, 184408 (2008).
- [28] W. G. Schmidt, S. Glutsch, P. H. Hahn, and F. Bechstedt, *Phys. Rev. B* **67**, 085307 (2003).
- [29] P. E. Blöchl, *Phys. Rev. B* **50**, 17953 (1994).
- [30] G. Kresse and D. Joubert, *Phys. Rev. B* **59**, 1758 (1999).
- [31] P. Vinet, J. Ferrante, J. H. Rose, and J. R. Smith, *J. Geophys. Res.* **92**, 9319 (1987).
- [32] G. P. Francis and M. C. Payne, *J. Phys.: Condens. Matter* **2**, 4395 (1990).
- [33] H. J. Monkhorst and J. D. Pack, *Phys. Rev. B* **13**, 5188 (1976).
- [34] K. E. Lipinska-Kalita, P. E. Kalita, O. A. Hemmers, and T. Hartmann, *Phys. Rev. B* **77**, 094123 (2008).
- [35] M. Marezio and J. P. Remeika, *J. Chem. Phys.* **46**, 1862 (1967).
- [36] F. Fuchs and F. Bechstedt, *Phys. Rev. B* **77**, 155107 (2008).
- [37] S. Geller, *J. Chem. Phys.* **33**, 676 (1960).
- [38] J. Ahman, G. Svensson, and J. Albertsson, *Acta Crystallogr. C* **52**, 1336 (1996).
- [39] *CRC Handbook of Chemistry and Physics*, 95th ed., edited by W. M. Haynes (CRC Press, London, 2014), pp. 4–5.
- [40] A. Schleife, F. Fuchs, J. Furthmüller, and F. Bechstedt, *Phys. Rev. B* **73**, 245212 (2006).
- [41] M. Yan-Mei, C. Hai-Yong, Y. Kai-Feng, L. Min, C. Qi-Liang, L. Jing, and Z. Guang-Tian, *Chin. Phys. Lett.* **25**, 1603 (2008).
- [42] J. P. Perdew, K. Burke, and M. Ernzerhof, *Phys. Rev. Lett.* **77**, 3865 (1996).
- [43] J. B. Varley, J. R. Weber, A. Janotti, and C. G. van de Walle, *Appl. Phys. Lett.* **97**, 142106 (2010).
- [44] G. Sinha, K. Adhikary, and S. Chaudhuri, *J. Cryst. Growth* **276**, 204 (2005).
- [45] L. Binet, D. Gourier, and C. Minot, *J. Solid State Chem.* **113**, 420 (1994).
- [46] P. Erhart, A. Klein, R. G. Egdell, and K. Albe, *Phys. Rev. B* **75**, 153205 (2007).
- [47] A. Navarro-Quezada, S. Alamé, N. Esser, J. Furthmüller, F. Bechstedt, Z. Galazka, D. Skuridina, and P. Vogt, *Phys. Rev. B* **92**, 195306 (2015).
- [48] B. C. Shih, Y. Xue, P. Zhang, M. L. Cohen, and S. G. Louie, *Phys. Rev. Lett.* **105**, 146401 (2010).
- [49] E. A. Albanesi, S. J. Sferco, I. Lefebvre, G. Allan, and G. Hollinger, *Phys. Rev. B* **46**, 13260 (1992).
- [50] J. F. Nye, *Physical Properties of Crystals: Their Representation by Tensors and Matrices* (Oxford University Press, Oxford, 1985).
- [51] B. Adolph, V. I. Gavrilenko, K. Tenelsen, F. Bechstedt, and R. Del Sole, *Phys. Rev. B* **53**, 9797 (1996).
- [52] H. H. Tippins, *Phys. Rev.* **140**, A316 (1965).
- [53] F. Fuchs, C. Rödl, A. Schleife, and F. Bechstedt, *Phys. Rev. B* **78**, 085103 (2008).
- [54] F. Bechstedt, K. Seino, P. H. Hahn, and W. G. Schmidt, *Phys. Rev. B* **72**, 245114 (2005).
- [55] M. Passlack, E. F. Schubert, W. S. Hobson, M. Hong, N. Moriya, S. N. G. Chu, K. Konstadinidis, J. P. Mannaerts, M. L. Schnoes, and G. J. Zyzdik, *J. Appl. Phys.* **77**, 686 (1995).
- [56] M. Rebien, W. Henrion, M. Hong, J. P. Mannaerts, and M. Fleischer, *Appl. Phys. Lett.* **81**, 250 (2002).
- [57] I. Bhaumik, R. Bhatt, S. Ganesamoorthy, A. Saxena, A. K. Karnal, P. K. Gupta, A. K. Sinha, and S. K. Deb, *Appl. Opt.* **50**, 6006 (2011).
- [58] *CRC Handbook of Chemistry and Physics*, 70th ed., edited by R. C. Weast (CRC, Boca Raton, FL, 1989), p. B-92.
- [59] C. Sturm, J. Furthmüller, F. Bechstedt, R. Schmidt-Grund, and M. Grundmann, *APL Mater.* **3**, 106106 (2015).